

Fitting Pulsar Wind Tori

C.-Y. Ng & Roger W. Romani

Department of Physics, Stanford University, Stanford, CA 94305

`ncy@astro.stanford.edu, rwr@astro.stanford.edu`

ABSTRACT

CXO imaging has shown that equatorial tori, often with polar jets, are very common in young pulsar wind nebulae (PWNe). These structures are interesting both for what they reveal about the relativistic wind itself and for the (nearly) model-independent measurement of the neutron star spin orientation they provide. The later is a particularly valuable probe of pulsar emission models and of neutron star physics. We describe here a procedure for fitting simple 3-D torus models to the X-ray data which provides robust estimates of the geometric parameters. An application to 6 PWN tori gives orientations, PWN shock scales and post-shock wind speeds along with statistical errors. We illustrate the use of these data by commenting on the implications for kick physics and for high energy beaming models.

Subject headings: stars: neutron – pulsars – stars: rotation

1. Introduction

The Crab nebula has long been known to have a subluminescent zone and termination shock surrounding its central pulsar. One of the striking successes of the *Chandra X-ray Observatory* (*CXO*) mission has been to show that this shock is likely an equatorial band and that similar structures are seen around a number of young pulsars (e.g. Weisskopf *et al.* 2000, Pavlov *et al.* 2001, Helfand, Gotthelf & Halpern 2001, Gotthelf 2001). Romani & Ng (2003) argued that the apparent symmetry of such PWNe, if interpreted as equatorial tori, allowed a robust fit for the 3-D orientation of the pulsar spin axis $\vec{\Omega}$ and showed that measurement of this axis can be effected even for quite faint PWNe. They also argued that, taking PSR J0538 + 2817 as an example, comparison of the spin axis with the proper motion axis \vec{v} can be a sensitive probe of pulsar physics (see Spruit & Phinney 1998, Lai *et al.* 2001). In particular, when the alignment is due to rotational averaging of the transverse momentum, tight alignments imply momentum kicks lasting many times the pulsar initial spin period. Such time constraints on the kick timescale can exclude otherwise plausible models. We wish here to systematize this compar-

ison by outlining how robust fits for model parameters can be obtained even for relatively low-count *CXO* PWN images.

The characteristic scale of the wind termination shock around a pulsar of spindown power \dot{E} is

$$r_T \approx (\dot{E}/4\pi c P_{ext})^{1/2}.$$

This structure should be azimuthally symmetric about the pulsar spin axis when $P_{ext} \geq P_{ram} = 6 \times 10^{-10} n v_7^2 \text{g/cm/s}^2$, i.e. when the pulsar is subsonic at speed $100 v_7 \text{km/s}$. Pulsars will seldom be sufficiently slow to show toroidal shocks in the general ISM (where they will have PWN bow shocks), but young PSR often satisfy the azimuthally symmetric torus condition in high pressure SNR interiors. van der Swaluw *et al.* (2003) have provided analytic descriptions of conditions in SNR interiors, modeling the pulsar parameters required for a subsonic PWN as the SNR evolves.

2. Fitting Model and Technique

The discovery papers showing obvious toroidal PWN structure have, of course, often provided estimates of the torus scale, position angle and inclination. However, most of these estimates were

simple eyeball matches or, at best 2-D fits of ellipses in the image plane. The ubiquity of clearly equatorial structures with toroidal symmetry and the robust physical interpretation in terms of a static termination shock in an equatorial wind argue that direct fits of the implied 3-D structure are most appropriate. Further, quantitative comparison with other pulsar observables requires error estimates for the geometric parameters, which are often not provided. Finally, we seek to constrain the orientations of central tori in PWNe, even when they are not immediately obvious. All of these considerations require a robust fitting procedure with (statistical) error estimates.

We adopt a default model of a simple equatorial torus with a Gaussian emissivity profile in cross-section. Clearly, this is not a sufficiently detailed model to describe the complete PWN structure in the highest resolution images. In fact, for Crab, Vela and a few fainter PWNe we find that multiple tori component significantly improve the model fits. Also, we do not fit the detailed radial variation of the torus emissivity and wind speed. Such extensions of the model could be useful for comparison with numerical models of relativistic shock flow (e.g. Komissarov & Lyubarsky 2003, Shibata *et al.* 2003). However, these models are far from complete, and for the fainter PWNe the existing count statistics do not warrant such model extensions. Accordingly we adopt the generic torus fit and apply this to six pulsars, with increasingly poor image statistics. Since for the bright PWNe fine structure beyond a simple torus is visible, we must assume that these models are incomplete descriptions of the fainter objects as well. However, the simple torus gives an adequate description of the data and, assuming that this model captures the gross nebular structure, we obtain quantitative estimates of the orientation and wind flow parameters. The estimates are quite robust to perturbations in the input fit assumptions. Note also that simpler structures are included as subsets of our fit parameter space, e.g. a simple uniform halo, which is reproduced by a face-on torus with small radius and large blur. Such models are strongly statistically excluded, even for the faintest sources.

We characterize the termination shock (torus) by a polar axis at a position angle Ψ ($0 - 180^\circ$, measured N through E), with inclination angle ζ ($0 - 180^\circ$) from the observer line of sight. The

torus is simply described by a radius r and a finite thickness or ‘blur’ of Gaussian cross section, dispersion δ , about the central ring. We assume that the surface brightness (averaged over its cross section) is uniform in azimuth. However, the post-shock flow is still expected to be mildly relativistic and so an azimuthally symmetric ring will vary in apparent intensity, due to Doppler boosting. Synchrotron emission of intensity I_0 and photon spectral index Γ in the rest frame will have an apparent intensity

$$I \propto (1 - \mathbf{n} \cdot \boldsymbol{\beta})^{-(1+\Gamma)} I_0$$

(Pelling, *et al.* 1987) where $\boldsymbol{\beta} = \mathbf{v}/c$ is the bulk velocity of the post shock flow and \mathbf{n} is the unit vector to the observer line of sight.

In practice we set up a coordinate grid with x , y oriented with the CCD frame and z along the observer line-of-sight. This is rotated to a grid aligned with the torus

$$\begin{aligned} x' &= -x \cos \Psi - y \sin \Psi \\ y' &= (x \sin \Psi - y \cos \Psi) \cos \zeta + z \sin \zeta \\ z' &= -(x \sin \Psi - y \cos \Psi) \sin \zeta + z \cos \zeta \end{aligned}$$

with x' along the line of nodes, and z' along the torus axis. In this frame the emissivity toward the Earth is

$$I(x', y', z') = \frac{N}{(2\pi\delta)^2 r} \times \left(1 - \frac{y' \sin \zeta}{\sqrt{x'^2 + y'^2}} \beta\right)^{-(1+\Gamma)} e^{-[z'^2 + (\sqrt{x'^2 + y'^2} - r)^2]/2\delta^2}$$

where N is normalized to the total number of counts in the torus component. We actually assume a fixed $\Gamma = 1.5$, typical of PWNe and leave β as a model parameter.

These parameters define the basic 3-D torus of PWN emission. To form the 2-D torus image for data fitting, we integrate the emissivity through the line of sight to get the counts in each pixel, i.e.

$$C(x, y) = \sum_z I(x', y', z')$$

The model image also generally includes a uniform background and a point source for the pulsar, whose intensity distribution is the PSF appropriate to the detector position and source spectrum. For Crab and Vela, the point sources have strong pile-up and we can optionally blank a small region

around the point source. There are a few special cases of this basic model. In several PWNe (most notably Vela), the termination shock has a double torus, presumably spaced above and below the spin equator. We model this with identical tori, symmetrically offset along the torus axis about the pulsar by distance d , following Helfand, Gotthelf & Halpern (2001). In the case of the Crab, the structure includes two, apparently inner and outer, tori. Finally in several cases relatively bright polar jets complicate the analysis. We can add model jet emission along the torus axis, blank the jet regions or include jet region photons as a fixed background. We do not at present fit these components separately but their inclusion makes for more appealing model images. The torus parameters are robust to the inclusion or exclusion of the ‘jet’ region photons.

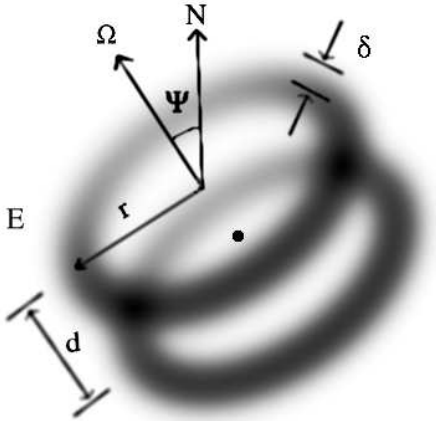


Fig. 1.— Torus Geometry – The figure is the plane of the sky projection of a double torus with fit parameters and angles labeled. ζ (not shown) is the angle between the sky plane normal (=the Earth line-of-sight \hat{z}) and $\vec{\Omega}$.

Thus the basic torus model includes parameters Ψ , ζ , r , δ , β and a background. Additional parameters can include the point source counts or double torus separation. To keep the model parsimonious, we apply the constraint that the total model counts $\Sigma_{xy} C_{xy}$ match the image counts (except for the Crab, where bright complex background structure is not adequately modeled by a constant background). Our fitting procedure uses maximum likelihood, with a merit function formed from the summed log probabilities of the observed

counts d_{xy} in each image pixel. We use Poisson statistics

$$P(d_{xy}) = \frac{C_{xy}^{d_{xy}} e^{-C_{xy}}}{(d_{xy}!)},$$

passing to Gaussian statistics for an expected pixel count $C_{xy} \geq 20$ in the CCD image. In this way the distribution of fluctuations in the fitted model parameters passes smoothly to χ^2 statistics in the limit of high count images. The merit function is minimized, using the simulated annealing package in Numerical Recipes (Press, *et al.* 1992). The initial parameter estimates are chosen by eye and the simplex generally relaxes quickly to the stable final solution, with a robust insensitivity to the initial conditions. The one exception is the blur thickness δ , which has a tendency to grow to absorb the unmodeled larger scale PWN enhancement present in many of the brighter nebulae. As this parameter is not particularly useful in the physical description of the shock, we fixed it at the initial (visual estimate) value in a number of cases. The other fit parameters are quite insensitive to δ over a broad range $\delta < r$.

Equally important are the parameter error estimates. We obtain these via fits to Monte Carlo Poisson realizations of the best fit-model. After 500 random simulations and fits we examine the distribution of the fit parameters. These distributions are well-behaved, with near-Normal distributions about the original fit parameters. We quote here 1- σ confidence intervals corresponding to 68% CL. These are projected (i.e. true multi-parameter) estimates of the statistical errors in the fit parameters. At very high confidence levels ($> 99\%$) the parameters become poorly constrained, especially for the fainter PWNe. Nevertheless we find that the estimated statistical errors are quite reliable well beyond 2- σ . Systematic errors, due to jets, complex backgrounds, or other unmodeled structures are of course not included, but these statistical estimates appear dominant for all but the brightest PWNe and thus provide useful estimates of the parameters of the *torus component* which captures the gross structure of the central PWN.

The simulations also reveal correlations between the fitting parameters. Ψ is, as expected, well decoupled from the other parameters. ζ and β are substantially co-variant with correlation coefficients as large as 0.7 since both affect the bright-

ness ratio between the front and back sides of the tori. Fluctuations toward large inclination thus have reduced β . Similarly for the PWNe with large inclinations, ζ and r are covariant (coefficient 0.3 to 0.7) since the projected angle of the torus' bright edge $r\cos\zeta$ is well constrained by the images. Our reported 1σ errors include these projected correlations.

Fit parameters and errors are reported for six PWNe with a range of brightness in Table 1. We start with the 'obvious' tori of Crab and Vela, continue with the 'apparent' tori of PSR J2229+6114 and PSR J1930+1852 and extend to two faint 'plausible' tori from pulsars for which existing estimates of the proper motion make spin axis measurements of particular interest. There are perhaps 10 additional PWN known where such analysis could be fruitful, and we expect there that several more useful torus measurements will be made as the *CXO* mission matures. In the present analysis, all images are from archival ACIS-S data sets, energy cut to 0.5-5keV. For the Crab we use ObsID 1998 (25ks), for Vela we combine ObsIDs 1987 and 2813-2820 (180ks). For the other objects we use the following observations: G54.1+0.3 (ObsID 1985, 40ks), PSR J2229+6114 (ObsID 2787, 100ks), PSR B1706-44 (ObsID 757, 15ks), PSR J0538+2817 (ObsID 2796, 20ks). We mention here special features of individual fits.

The two Crab tori are fitted sequentially, with the outer torus fitted first and then used as a fixed background for the inner torus fits. The model shown combines both components. The fitted tori are close to co-planar and have very small statistical parameter errors due to the high image counts. The Vela tori are spaced symmetrically about the pulsar, centered along the symmetry axis; we quote the value d in arcseconds projected on the sky. For the Crab and for Vela, the high S/N images show complicated fine detail in the tori and unmodeled fainter structures in the surrounding PWN. We have tested the fit sensitivity to these structures by, eg. blanking the jet regions, adjusting the blur thickness and shifting starting fit parameters. We find surprisingly small sensitivity to these changes in the torus fits: the fit values are quite robust, although clearly the very small statistical errors will be dwarfed even by the modest systematic biases.

For SNR G54.1+0.3 and PSR B1706-44, the

global minima of the merit functions pull the tori to small radii to absorb excess counts in the PSF wings of the central pulsar. By excluding torus count contributions to the merit function for pixels at $< 2''$, we obtain the minima listed in the table, which match the visual structure of the nebulae. PSR B1706-44 also has bright regions above and below the fit torus, which can be interpreted as polar jets and which produce a modest fraction of the counts attributable to the putative torus. To minimize the sensitivity of the torus fit to these 'jet' photons, we add these counts as a fixed background in the model, as can be seen in the corresponding model image.

The PWN of PSR J0538+2817 is quite faint, providing only $\sim 2\%$ of the point source counts. Accordingly, the geometry of the torus is sensitive to the amplitude of the PSF, and so the point source normalization cannot be fitted simultaneously. Instead the PSF amplitude is first fitted in the central $1''$. This (pile-up corrected) PSF is held fixed during the torus fitting. Consistency is checked by re-fitting for the point source in the presence of the torus background, confirming that the amplitude is unaffected. Romani & Ng (2003) have previously described this PWN, arguing that the spatial and spectral distinction from the PSF wings make the nebula highly significant, despite its low count rate. The fit errors in Table 1 are slightly larger than those in Romani & Ng (2003), because of the additional fit parameters and the multi-dimensional errors. In particular, slightly smaller errors ($\sim 6^\circ$ vs. $\sim 8^\circ$) can be obtained by direct fits to Ψ alone. However, an equatorial extension of the PWN is strongly required in the fit, the Ψ estimate remains robust to perturbations of the starting conditions and a simple uniform halo (small ζ) is strongly excluded – the figure of merit degrades to the 3.6σ level, referenced to our multi-parameter error flags, for models with $\zeta \approx 0$.

3. Application of Fit Parameters and Conclusions

In our fitting, we find that (for ζ not too small) the position angle Ψ is the most robust parameter. We believe that even if the simple torus model is inadequate to fully describe all nebulae, this measurement of the position angle of transverse PWN extension is very robust. Thus comparison of the

projected fit axis with the proper motion axis remains an important application. For Crab, the Caraveo & Mignani (1999) HST measurement of the Crab proper motion lies at $\Psi_{PM} = 292 \pm 10^\circ$. This is 12° or 1.2σ off of our inner ring axis. Similarly for Vela, we compare with the new radio interferometric proper motion of Dodson, *et al.* (2003) at $\Psi_{PM} = 302 \pm 4^\circ$, which has both higher astrometric accuracy and a corrected treatment of Galactic rotation effects from earlier optical estimates. This vector lies 8.6° from our fitted torus axis, a $\sim 2.1\sigma$ discrepancy. Several other comparisons are semi-quantitative at present; we discuss these below.

Neither PSR J1930+1852 in G54.1+0.3 nor PSR J2229+6114 in G106.3+27 has a directly measured proper motion. Further, these SNR are complex with no clear shell structure, so a velocity vector has not been estimated from an offset birth site. In contrast, Dodson & Golap (2002) and Bock & Gvaramadze (2002) have re-examined the controversial association between PSR B1706-44 and G343.1-2.3, and argued that this partly shell-like SNR is larger than previously believed, placing the pulsar well in the interior and making the association more plausible. The former authors find a southern extension suggesting a more complete circular shell; the vector from the center of this structure is at $\Psi_{PM} \sim 150^\circ$. The latter authors suggest a proper motion parallel to the expansion of the nearby bright shell rim, $\Psi_{PM} \sim 170^\circ$. These position angles are $\sim 10 - 20^\circ$ from our fit axis, but since the SNR evidently suffered asymmetric expansion, both of these geometrical estimates are uncertain. Thus while the axes are in general agreement, a direct measurement of the proper motion is essential for any serious comparison. PSR J0538+2817, in contrast, resides in S147 which has a quite symmetrical structure. Romani & Ng (2003) estimated a proper motion axis from the offset at $-32 \pm 4^\circ$, i.e. $< 1\sigma$ off of the PWN axis measured here. Kramer, *et al.* (2003) have recently managed to extract a timing proper motion for this pulsar which confirms the association with S147, although the PA is poorly determined. Here, both higher statistics X-ray imaging and an astrometric proper motion are needed to effect a precision test.

There are two other young pulsars in shell SNR with recent proper motion measurements, PSR

B1951+32 in CTB80 and PSR B0656+14 in the Monogem Ring. Pulsar B1951+32 has a proper motion at $\Psi_{PM} = 252 \pm 7^\circ$ away from its SNR birthsite (Migliazzo *et al.* 2002) and is presently interacting with the dense swept-up shell. Thus the prominent bow shock seen in HST imaging is not unexpected; one would not expect a toroidal wind shock. It is plausible that a ‘jet’ wind could punch through the bow shock and Hester (2000) has proposed that the H α ‘lobes’ bracketing the bow shock mark the pulsar polar jets. Under this interpretation we measure the spin axis is at $\approx 265 \pm 5^\circ$, which is 13° ($\sim 1.4\sigma$) away from the proper motion axis.

With a new parallax distance measurement Briskin, *et al.* (2003) and Thorsett, *et al.* (2003) find that PSR B0656+14 is enclosed within the ~ 66 pc-radius Monogem ring. The surprisingly small proper motion at $\Psi_{PM} = 93.1 \pm 0.4^\circ$ implies a transverse velocity of only 60km/s. If the pulsar has a more typical ~ 500 km/s space velocity, it must be directed along the Earth line-of-sight; indeed, the parallax distance is consistent with the near side of the Monogem ring. At its characteristic age, the pulsar should still be within the remnant interior for radial velocities as large as ~ 600 km/s. This SNR exploded in the low density local ISM, so we expect the PWN to be toroidal with a characteristic radius of $\sim 3''$. Interestingly, a short *CXO* observation shows a faint, nearly circular halo around the pulsar at this scale (Pavlov, *et al.* 2002), suggesting a face-on torus. Scheduled *CXO* observations have the sensitivity to map this structure, which we predict will be consistent with a torus tilt of $\sim 15^\circ$.

Table 2 collects the projected proper motion and spin-axis position angle (\vec{v} , $\vec{\Omega}$) estimates along with estimates of the line-of-sight inclination for these young pulsars. The trend toward alignment (small $|\Delta\Psi_{\Omega-v}|$) is strong, albeit imperfect. Formally, one should impose a prior on the maximum total space velocity v before evaluating the likelihood of a position angle range $\{\Delta\Psi\}$. If the 3-D angle between \vec{v} and the projected position angle is θ , then a physical upper limit on the plausible $v = v_\perp \cos\theta / \cos\Psi$ restricts the allowed range of θ . However, in practice all of these pulsars have relatively small $v = v_\perp$, so the disallowed range is negligible and the probability of a position angle range is simply $2(\Delta\Psi_{max} - \Delta\Psi_{min})/\pi$.

If only the 1σ maximum $|\Delta\Psi|$ are considered, then for Crab and Vela alone, there is a 3% chance of obtaining alignments as close as those seen from isotropically distributed \vec{v} , $\vec{\Omega}$. However if the other three angle estimates of Table 2 are included, the chance probability falls to 0.04%. On the other hand, the weighted combination of these measurements gives $\langle|\Delta\Psi_{\Omega,v}|\rangle = 10.0 \pm 2.7^\circ$, significantly different from 0. This finite misalignment probes the characteristic timescale of the neutron star birth kick, adopting the Spruit & Phinney (1998) picture of rotational averaging. As discussed in Romani & Ng (2003), the kick timescale constraints are very sensitive to the initial spin periods of the individual pulsars. We defer a detailed comparison with kick models to a later communication.

A reliable measurement of the spin axis inclination ζ can also be particularly valuable for these young pulsars. Many of these objects are high energy (hard X-ray and γ -ray) emitters and the modeling and interpretation of the pulse profiles is quite sensitive to ζ (Romani & Yadigaroglu 1995). Radio techniques (polarization sweeps and pulse width fitting) are often used to estimate ζ , but these are subject to substantial interpretation uncertainties. For example polarization sweep results are affected by 90° mode jumps in various pulse components, which can often only be resolved with single pulse studies. Perhaps this complexity is not surprising, since the radio emission, at relatively low altitude, is sensitive to higher order multipoles and the details of the magnetic polar cap structure. In the wind zone all such details are likely lost. If high energy emission is generated in outer magnetosphere ($\sim 0.1 - 0.3r_{LC}$) gaps, then since r_{LC}/r_{NS} is large, high order multipoles should die away and the pulse profiles should be sensitive only to magnetic inclination and ζ .

We list some radio inclination estimates in Table 2 – however we caution that substantially different values are available in the literature for many of these pulsars. For Crab and PSR J0538+2817 the agreement with our fit ζ appears good. For Vela and PSR B1706-44 the discrepancies are large. Interestingly, Helfand, Gotthelf & Halpern (2001) match the axis ratio of the projected PWN torus by eye and find $\zeta = 55^\circ$ in good agreement with the radio estimate; however this value is very strongly excluded in our fits.

Our relative ζ s for Vela and PSR B1706-44 do however make sense in the outer magnetosphere picture (Romani & Yadigaroglu 1995), with PSR B1706-44 at smaller ζ producing a narrower double γ -ray pulse and a larger phase delay from the radio. We can further make some predictions for objects not yet observed at γ -ray energies. If our PWN ζ estimates hold up, we would expect γ -ray emission from PSR J2229+6114 to show a merged double pulse, somewhat narrower than that of PSR B1706-44 (as appears to be the case in the hard X-ray), while PSR J0538+2817 should show a wide, Vela-like double pulse. PSR J1930+1852 in G54.1+0.3 may be very faint in the γ -ray since its small $180^\circ - \zeta = 33^\circ$ suggests that any outer-magnetosphere γ -ray beams miss the Earth line-of-sight. Finally PSR B0656+14 which is many times fainter in $> 100\text{MeV}$ γ -rays than expected from its spin-down luminosity is widely believed to be viewed nearly pole-on. In this orientation the strong outer-magnetosphere γ -ray beams would not be visible, although we should see γ emission from the pair production fronts in the radio zone above the polar cap. New *CXO* imaging may allow a quantitative fit to the PWN, supporting the apparent small ζ .

Also physically interesting are the estimates for the post-shock velocities β . For the Crab nebula, our fit value compares well with the $\beta \sim 0.5$ found for the motions of wisps near the torus (Hester, *et al.* 2002), although clearly our very small statistical fit errors must under-predict the true uncertainty. Moreover, it is puzzling that we get slightly larger β for the outer ring. One certainly expects the flow speeds to drop rapidly in the outer nebula and *CXO/HST* data do show pattern velocities as small as $\beta \sim 0.03$ in the outer parts of the X-ray nebula. For Vela, no estimates of β from torus motions have yet been published, but Pavlov, *et al.* (2003) find $\beta \sim 0.3-0.6$ for features in the outer jet, which bracket the torus β found here. The interpretation of the outer jet speed is apparently complicated by a varying orientation with respect to the line of sight. Likely the inner jet/counter-jet provide a cleaner comparison with the torus β ; several authors have noted the larger counter-jet brightness suggests that it is approaching the observer. Using the time-averaged image in Figure 1, measuring a $5''$ length equidistant from the pulsar on each jet and subtracting

the interpolated background from either side, we find a counter-jet/jet count ratio $f_B = 2.3$. For a continuous, time-average jet of photon index Γ the the Doppler boosting ratio is

$$f_B = [(1 + \beta \cos \zeta)/(1 - \beta \cos \zeta)]^{\Gamma+1}$$

(the power $\Gamma + 2$ applies for isolated bright blobs). Pavlov, *et al.* (2003) report a inner jet spectral index $\Gamma \approx 1.1$, which with our fit ζ gives $\beta_J = 0.45$, in remarkably good agreement with our torus β . It is worth noting, however, that even these inner jets show significant variation, so a time-resolved study of pattern speeds and brightness is likely needed for a precise jet β .

No clear pattern yet emerges from the β estimates presented here, although there is a weak anti-correlation between the light cylinder magnetic field and β (correlation coefficient ≈ -0.3). If significant, this may suggest an anti-correlation between pair multiplicity, expected to be large in the narrow gaps of high \dot{E} , short period pulsars, and the wind speed. Ultimately, comparison of β in different PWN components at different latitudes, and between PWNe, promises to become an important new probe of pulsar electrodynamics.

For Vela, and a few fainter objects, the presence of a double ring already suggests some increase in pair multiplicity away from latitude 0° . If we deproject the ring separation as seen from the pulsar, we get a brightness peak (mid-plane of the torus) at co-latitude

$$\theta_{\text{Tor}} = \tan^{-1}(2r \sin \zeta / d) \approx 74^\circ.$$

This is about 10° larger than our best fit ζ . For Vela, the polarization sweep rate maximum suggests a magnetic axis impact angle $\beta = \zeta - \alpha = -4^\circ$. Notice that this is on the same side of the line-of-sight ($\alpha > \zeta$) as our fit torus. Thus we might plausibly associate the two tori with a near-radial outflow of high pair multiplicity plasma from the magnetosphere open zones. Perhaps further observation and modeling could distinguish between pairs produced in a vacuum gap near the star surface (polar cap) with plasma produced in an outer magnetosphere gap above the null-charge surface. For example, the outer magnetosphere gaps should populate field lines at angles $> \alpha$, consistent with the observed $\theta_{\text{Tor}} > \alpha$. If α is close to $\pi/2$ (e.g. Crab, PSR J0538+2817) the pair plasma

from the two poles should merge, leading to a single thicker torus.

In conclusion, the ubiquitous azimuthally symmetric torus (+jet) structures seen about young pulsars provide an important new probe of the viewing geometry. We have described a procedure for fitting simple geometric models to X-ray images that match the gross structure of the central regions of many PWNe and provide robust estimates for model parameters. These models clearly do not capture all of the rich, and dynamic, structural details seen in the brighter nebulae, such as Crab and Vela. However the fitting procedure does reduce biases of by-eye ‘fits’ and does allow extraction of geometrical parameters from quite faint objects. Accordingly, such fits should allow us to measure spin axis orientations for a larger set of pulsars and use these angles to probe models of the neutron star kick and of pulsar magnetospheric physics.

This work was supported in part by CXO grant G02-3085X. We thank Walter Briskin for discussion of recent pulsar astrometry.

REFERENCES

- Bock, D.C.-J. & Gvaramadze, V.V. 2002, A&A394, 533
- Briskin, W., Thorsett, S.E., Golden, A. & Goss, W.M. 2003, AJ, in press
- Caraveo, P.A. & Mignani, R.P. 1999, A&A, 344, 357
- Dodson, R. & Golap, K. 2002, MNRAS, 334, L1
- Dodson, R., Legge, D., Reynolds, J.E. & McCulloch, P.M. 2003, astro-ph/0302374
- Gotthelf, E. V. 2001, AIP Conference Proceedings 586, "Relativistic Astrophysics: 20th Texas Symposium." Ed. Wheeler and Martel (Austin, Tx); astro-ph/0105128
- Helfand, D.J., Gotthelf, E.V. & Halpern, J.P. 2001, ApJ, 556, 380
- Hester, J.J. 2000, BAAS, 97.8216
- Hester, J.J. 2002, ApJ, 557, L49

- Komissarov, S.S. & Lyubarsky, Y.F. 2003, MNRAS, 344, L93
- Kramer, M., *et al.* 2003, ApJ, 593, L31
- Krishnomohan, S. & Downs, G.S. 1983, ApJ, 265, 372
- Lai, D., Chernoff, D.F. & Cordes, J.M. 2001, ApJ, 549, 1111
- Lyne, A.G. & Manchester, R.N. 1988, MNRAS, 234, 477
- Migliazzo, J.M., *et al.* 2002, ApJ, 567, L141
- Pavlov, G.G., Kargaltsev, O.Y., Sanwal, D. & Garmire, G.P. 2001, ApJ, 554, L189
- Pavlov, G.G., Zavlin, V.E. & Sanwal, D. 2002, in Proc. of 270th Heraeus Symp, 273.
- Pavlov, G.G., Teter, M., Kargeltsev, O. & Sanwal, D. 2003, ApJ, 591, 1157
- Pelling, R.M. *et al.* 1987, ApJ, 319, 416
- Press, W.H., Flannery, B.P., Teukolsky, S. & Vetterling, W. 1992, *Numerical Recipes* (Cambridge University Press:Cambridge).
- Romani, R.W. & Yadigaroglu, I.-A. 1995, ApJ, 438, 314
- Romani, R.W. & Ng, C.-Y. 2003, ApJ, 585 L41
- Shibata, S., *et al.* 2003, MNRAS, in press.
- Spruit, H. & Phinney, E.S. 1998, Nature, 393, 139
- Thorsett, S.E., *et al.* 2003, ApJ, 592, L71
- van der Swaluw, E., Achterberg, A., Gallant, Y.A., & Keppens, R. 2003, A&A, 397, 913
- Weisskopf, M.C. *et al.* 2000, ApJ, 536, L81

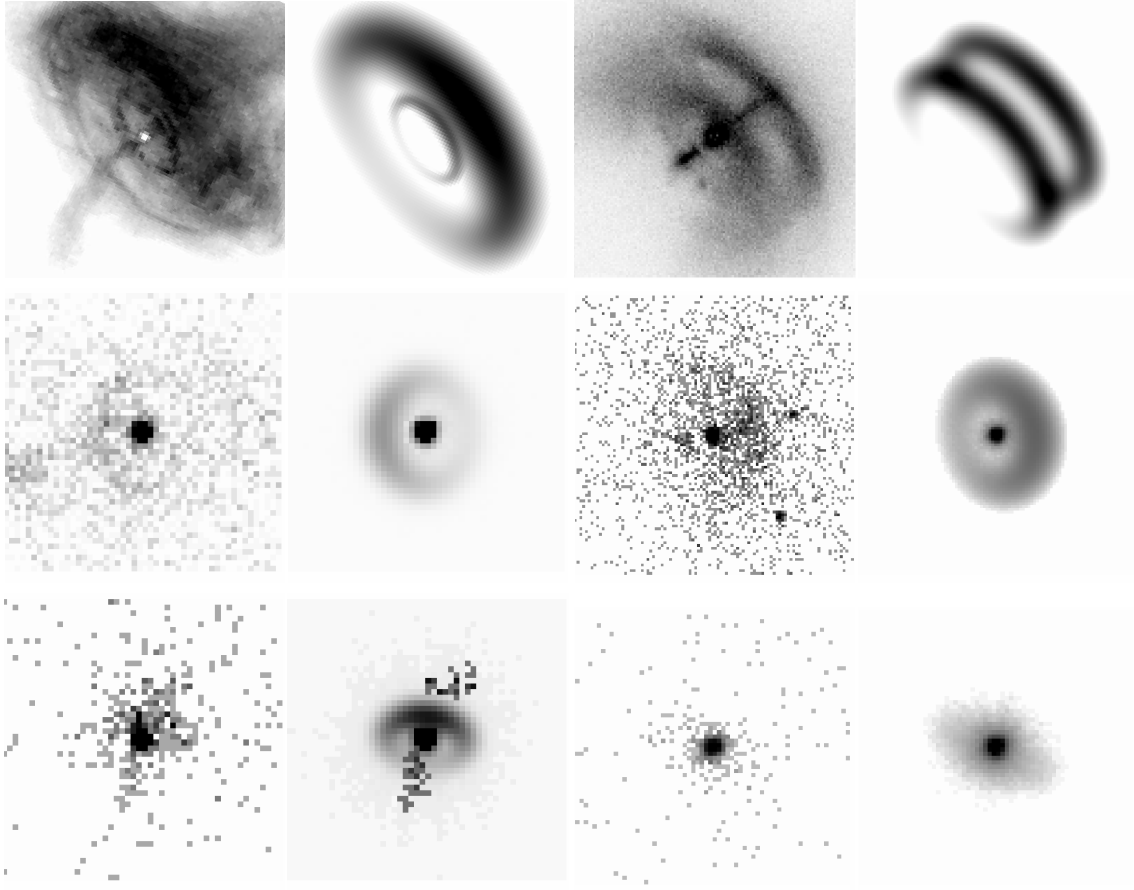


Fig. 2.— Pulsar Wind Tori – *CXO* ACIS images (left) and best-fit models (right) for Crab, Vela, G54.1+0.3, PSR J2229+6114, PSR B1706-44 and PSR J0538+2817 (left-right, top-bottom).

TABLE 1

object	ψ	ζ	r''	δ	β	PS/torus	sep''
Crab (inner)	$124.0^{+0.1}_{-0.1}$	$61.3^{+0.1}_{-0.1}$	$15.60^{+0.03}_{-0.03}$	3.0*	$0.490^{+0.005}_{-0.006}$	$-/1.0 \times 10^5$	-
Crab (outer)	$126.31^{+0.03}_{-0.03}$	$63.03^{+0.02}_{-0.03}$	$41.33^{+0.02}_{-0.03}$	5.9*	$0.550^{+0.001}_{-0.001}$	$-/1.1 \times 10^7$	-
Vela	$130.63^{+0.05}_{-0.07}$	$63.60^{+0.07}_{-0.05}$	$21.25^{+0.03}_{-0.02}$	3.0*	$0.44^{+0.004}_{-0.003}$	$-/1.3 \times 10^6$	$11.61^{+0.03}_{-0.03}$
SNR G54.1+0.3	91^{+4}_{-5}	147^{+3}_{-3}	$4.6^{+0.1}_{-0.1}$	$1.1^{+0.1}_{-0.1}$	$0.62^{+0.04}_{-0.03}$	1701/602	-
PSR J2229+6114	103^{+2}_{-2}	46^{+2}_{-2}	$9.3^{+0.2}_{-0.2}$	2.5*	$0.49^{+0.02}_{-0.02}$	2221/1113	-
PSR B1706-44	175^{+3}_{-4}	55^{+3}_{-3}	$3.5^{+0.2}_{-0.1}$	0.74*	$0.65^{+0.03}_{-0.04}$	384/168	-
PSR J0538+2817	155^{+8}_{-8}	99^{+8}_{-8}	$6.3^{+1.0}_{-0.7}$	$1.7^{+0.3}_{-0.7}$	$0.54^{+0.09}_{-0.08}$	2442*/52	-

* = held fixed in the global fit.

TABLE 2
PROPER MOTION AND SPIN AXIS ANGLES

<i>Pulsar</i>	Ψ	Ψ_{PM}^\dagger	$ \Delta\Psi_{\Omega.v} $	ζ	ζ_R
B0525+21	124.0 ± 0.1	292 ± 10	12 ± 10	61.3 ± 0.1	62^a
B0656+14	—	93.1 ± 0.4	—	small	16^b
J0538+2817	155 ± 8	$328 \pm \sim 4$	7 ± 9	99 ± 8	97^c
B0833-45	130.6 ± 0.1	302 ± 4	8.6 ± 4	63.6 ± 0.1	56^d
B1706-44	175 ± 4	$160 \pm \sim 10$	$15 \pm \sim 11$	55 ± 0.2	75^e
B1951+32	$85 \pm \sim 5$	252 ± 7	$13 \pm \sim 9$	—	—

References: \dagger see text, a see Romani & Yadigaroglu (1995), b Lyne & Manchester (1988), c Kramer, *et al.* (2003), d Krishnamohan & Downs (1983), e S. Johnston, priv. comm.